

CLAS-Note-91-005

March 6, 1991

**PLASTIC SCINTILLATOR AND WAVELENGTH SHIFTER TESTS
FOR THE CLAS ELECTROMAGNETIC CALORIMETER**

V.D. Burkert¹, P. Degtyarenko², K. Egiyan³, S. Majewski¹
S. Marekhin⁴, M. Ohanjanyan³, Yu. Sharabyan³, R. Wojcik¹

ABSTRACT

Light transmission and time resolution measurements of long strips of plastic scintillators are discussed. The effect of wavelength shifter readout on the time resolution is discussed as well.

¹ CEBAF, Newport News, Virginia 23606, USA

² Institute for Theoretical and Experimental Physics, Moscow, USSR

³ Yerevan Physics Institute, Yerevan, USSR

⁴ Institute of Physics and Technology, Kharkov, USSR

1. Introduction

The forward region of the six CLAS detector sections, corresponding to scattering angles between $\sim 5^\circ$ and 45° , will each be equipped with an electromagnetic calorimeter (EMC) of the lead/scintillator 'sandwich' type.

The calorimeters are an integral part of the CLAS detector system. They are particularly important in identifying both charged and neutral particles. For example:

- In electron scattering experiments, the EMC will be used in conjunction with the threshold gas Cerenkov counters for electron and pion identification over an energy range of 0.5 to 4(6) GeV. By properly tagging pions, one can greatly reduce background due to misidentified electron triggers. EMC based background suppression is available both at the data acquisition trigger level and later at the more refined analysis level.
- The EMC will be used in the reconstruction of π^0 and η events via detection and reconstruction of their 2γ decays, and in the detection of radiative photons.
- The EMC will also be used for the detection of neutrons and the discrimination between photons and neutrons.

The design, requirements, and expected performance of the EMC are described in the CEBAF "Conceptual Design Report on Basic Experimental Equipment"⁽¹⁾ A sketch of the one of the six calorimeter modules is shown in Figure 1. The maximum scintillator strip length is about 430 cm. Clearly, in order to achieve a uniform response over the entire area covered by the EMC, scintillator bars with excellent light transmission properties are needed. Uniform response is particularly important for triggering. Any non-uniformity in the calorimeter response will result in an increased trigger rate at a given nominal energy threshold.

We have tested long plastic scintillator bars from Bicron Corporation* and from NE Technology** of various lengths and thicknesses. The wavelength shifter bars (WLS) tested were ordered from NE Technology. The

* Bicron, Newbury, Ohio 44065

** NE Technology Ltd., Sighthill, Edinburgh EH11 4BY, Scotland

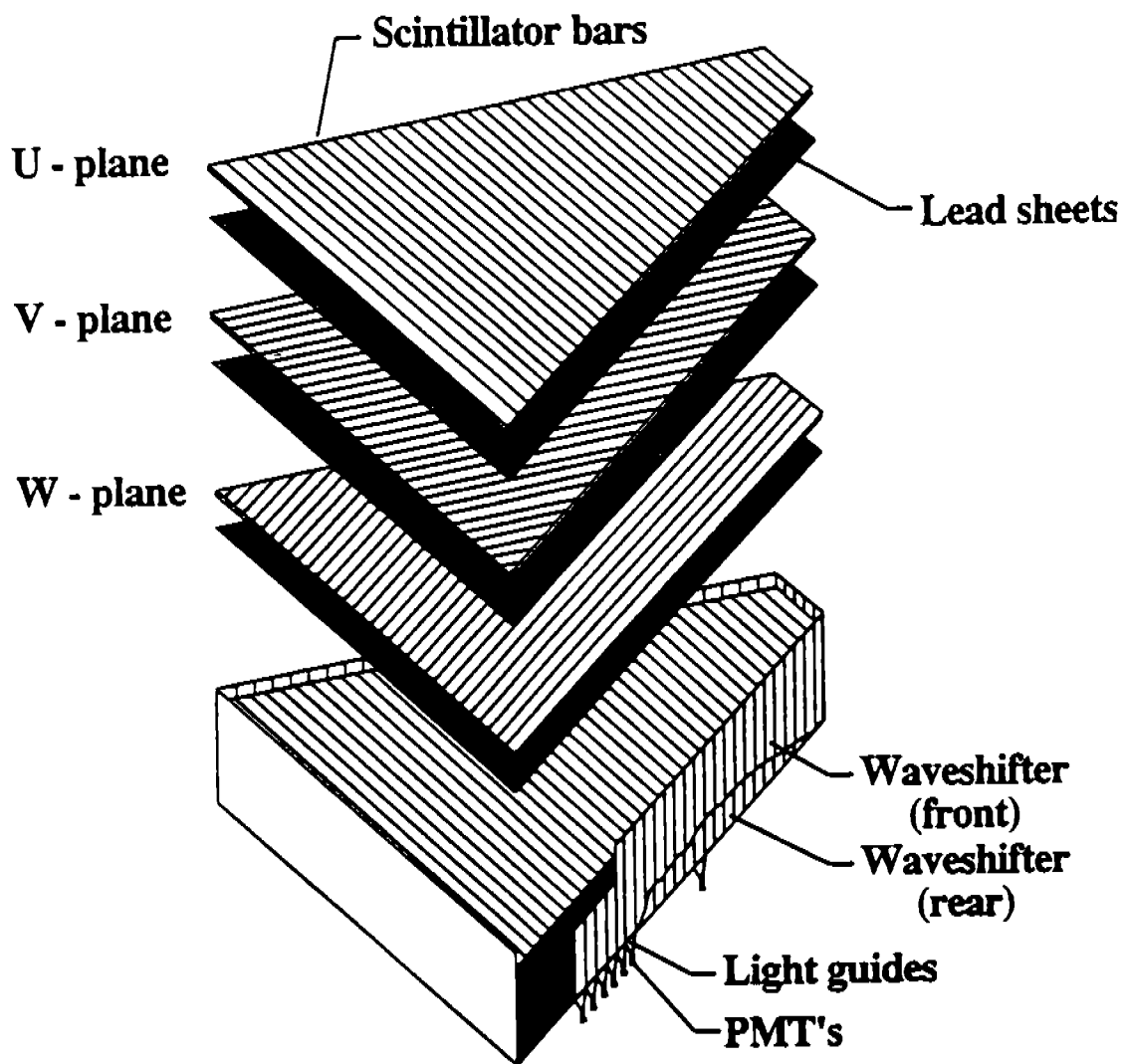


Figure 1: *Sketch of one of the six CLAS electromagnetic calorimeter modules (exploded view).*

dimensions of the scintillator and WLS bars are listed in table 1. In this note we report about test measurements for the 1 cm thick strips only.

2. Experimental Setup

The apparatus used in the scintillator tests is shown in Figure 2. A 5 meter long, light-tight box was constructed, which housed the plastic scintillator bars, the photomultipliers, and the radioactive source. The two ends of the scintillator bars were readout by XP2262 photomultipliers* equipped with CERN made bases. These bases were especially designed for use with this type of PMT. In the setup 1, used in the attenuation measurements, the scintillator light was transmitted to the photomultiplier at the right end via a small (~ 1 mm) air gap. Light generated in the scintillator bars was also detected by the probe PMT located on the opposite side of the scintillator bar with its photocathode facing the radioactive source. The distance of the probe PMT to the scintillator surface was 30 ± 1 mm and was measured to ~ 0.2 mm along the entire length of the scintillator for solid angle corrections. The relative systematic error for measurements from point to point is about 5%.

This setup allowed establishment of a strict time and amplitude correlation between the PMT signals.

In the setup 2, which was used for the WLS light transmission tests, the radioactive source was attached to a small piece of scintillator (probe scintillator) located between the probe PMT and the wave shifter bar. This way the light generated in the probe scintillator was not only viewed by the probe PMT, but was also (partially) transmitted to the waveshifter bar, and read out by a PMT attached to one end of the waveshifter.

In either setup, the radioactive source and the probe PMT were mounted on a cart that could be moved along the scintillator or waveshifter bar to be tested. Signals from the probe counter were registered in coincidence with signals from the PMT attached to the right end of the scintillator bars. The anode signals were fed into fast, leading edge discriminators with low threshold (10 mV) for the right and left PMT, and variable threshold (50 - 750 mV) for the probe. The discriminator outputs were brought to CAMAC TDC's with 50 psec resolution. The (inverted) dynode signals were directly fed into charge integrating ADC's. The source (^{87}Ru) emitted electrons with an energy spectrum ranging up to energies of 3.5 MeV.

* Philips Corporation, France

Vendor	Material	Type	Length (cm)	Thickness (cm)	Amount
NE	Scintillator	NE110	310	1.0	3
	Scintillator	NE110	310	0.6	3
	Waveshifter	NE172	50	1.0	2
Bicron	Scintillator	BC412	400	1.0	4
	Scintillator	BC412	400	0.6	2

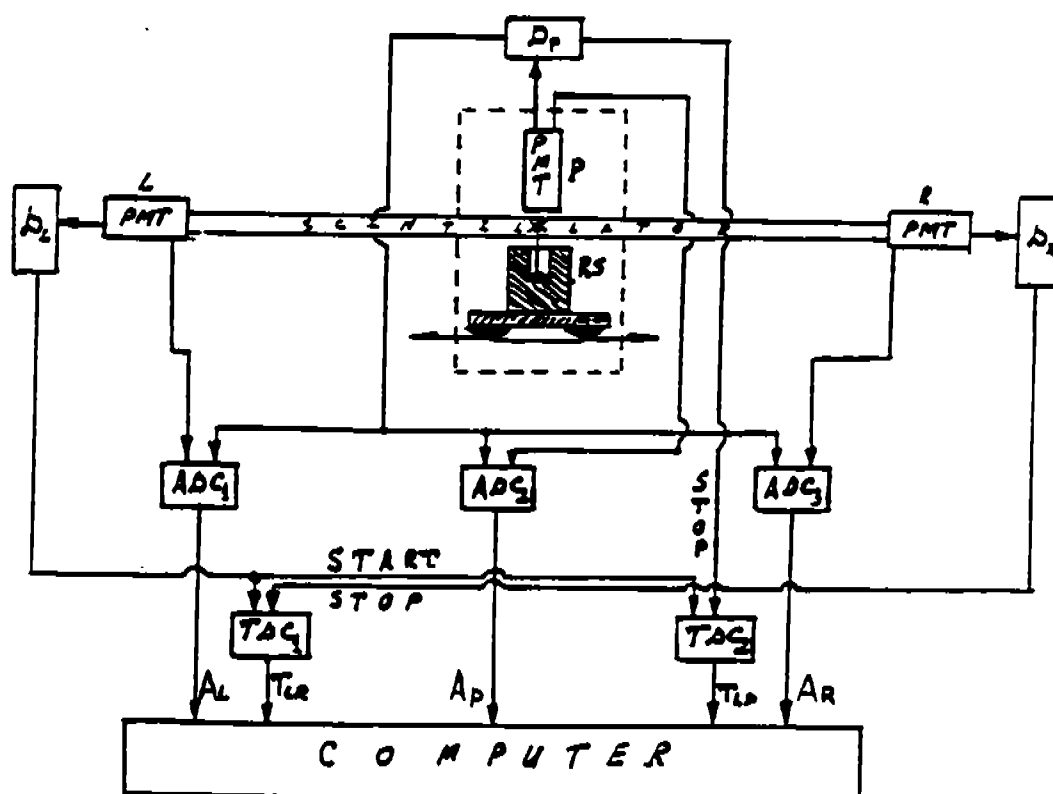


Figure 2: Schematic outline of the test setup. (D - Discriminator; L - Left; R - Right; P - Probe; RS - Radioactive Source)

3. Energy Calibration

Cosmic rays were used in order to establish the relation between energy deposited in the scintillator and the number of photoelectrons observed in the PMT. Towards this end the pulseheight distribution for cosmic was measured with the probe counter positioned close to the readout side of the scintillator strip. An additional scintillation counter was placed below the long scintillator strip opposite to the probe PMT, and used in conjunction with the probe counter to select cosmic muons penetrating the scintillator approximately perpendicular to the surface. Figure 3 shows the pulseheight distribution measured in the probe counter. The peak position corresponds to approximately 2 MeV energy deposition in the long scintillator. The absolute systematic uncertainty of the energy calibration is estimated to $\sim 30\%$, whereas relative systematic errors in the determination of the mean value for different measurements are estimated to $\sim 15\%$.

4. Attenuation Measurements of Scintillators

For these measurements the radioactive source was used. The pulseheights in the PMT's were registered every 20 cm along the scintillator bars. Figure 4 shows a typical ADC spectrum, for different positions along the scintillator, and corrected for pedestals. In these spectra, pulseheight cuts were applied to the probe PMT to select a well defined energy deposition in the scintillator bars corresponding to $dE/dx = 2.0 \pm 0.3 \text{ MeV}$. Various parametrizations to fit the spectra were tried. It turned out that using Poisson-like distributions and Gauss distributions gave nearly the same results for the mean values. Poisson fits gave better chisquared (χ^2/NDF from 1 to 2) which made parametrisation more stable. Therefore Poisson distributions were used in the final analysis. The light transmission properties of the scintillators were measured under the following condition:

- one end viewed by a 2" PMT* via a 1 mm air gap.
- away side end covered with black tape attached to the scintillator using optical grease.

The black tape was used to avoid light reflection at the away side end (up to 20% of light is reflected if this end is left open).

The CERN PAW package^[2] was employed in this analysis. The measured x-dependencies of mean pulseheights obtained from the Poisson fits for

* Philips XP2262

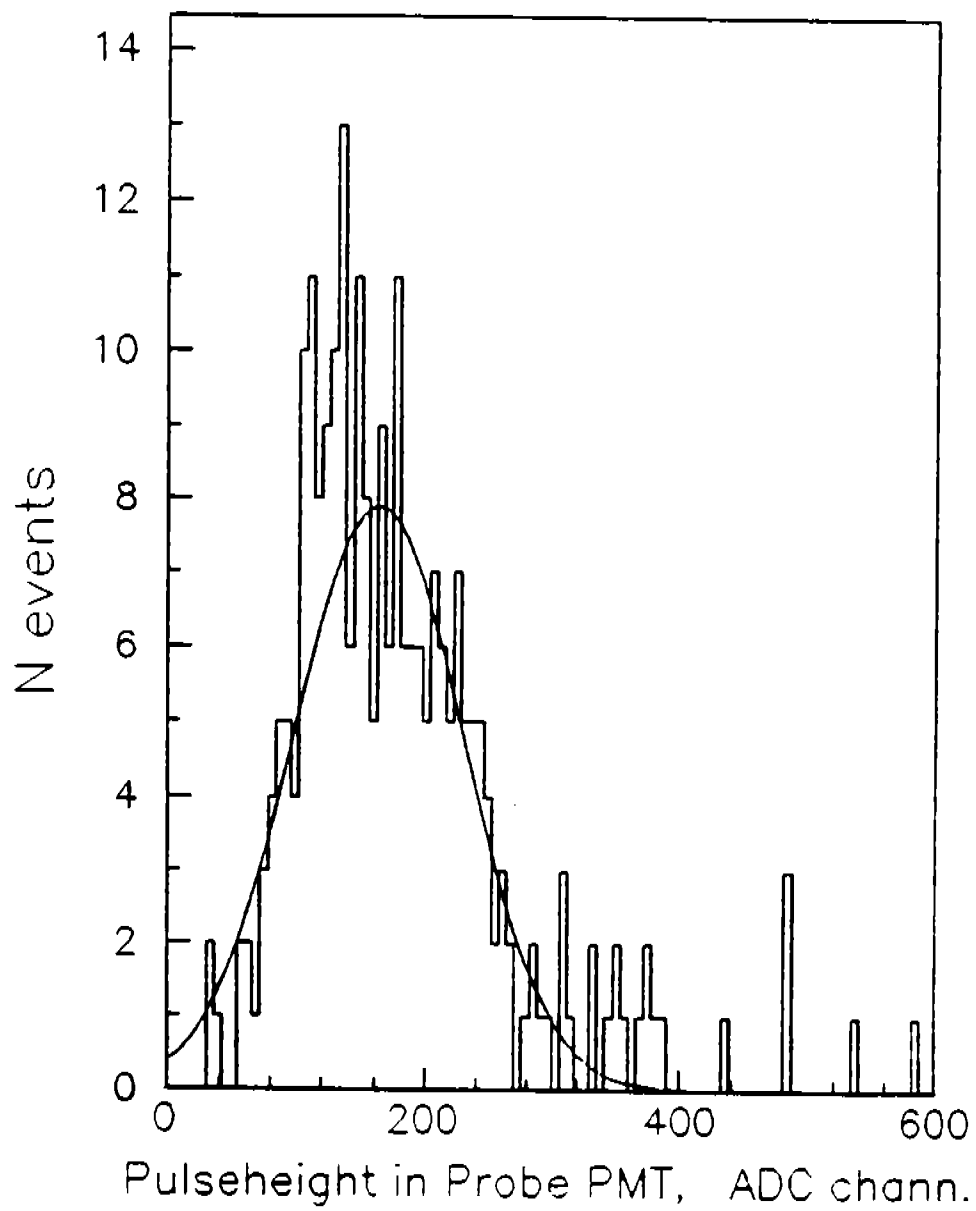


Figure 3: *Pulseheight distribution in the probe PMT for cosmic muons.*

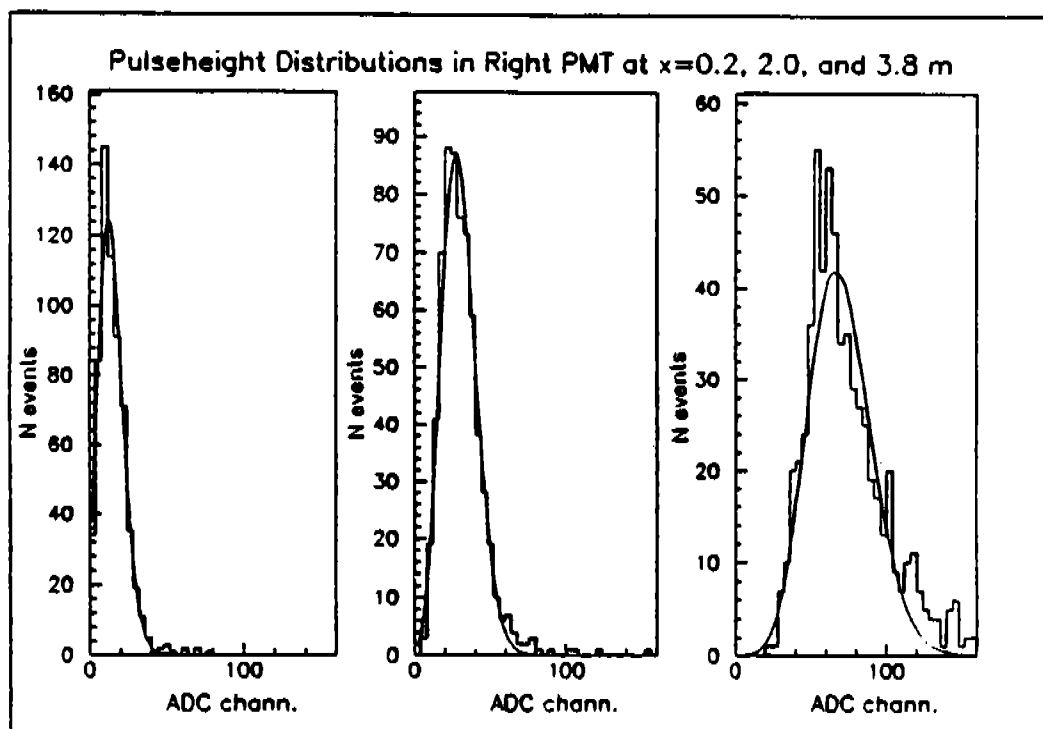


Figure 4: Typical pulseheight spectra. $x = 0.20 \text{ m}$, 2.0 m , and 3.8 m indicate the position along the scintillator measured from the left end. The solid lines represent fits to a Poisson distribution.

the different scintillators are shown in Figure 5. Averages over three of the 4 m and all of the 3.1 m long strips are displayed. $A_r(x)$ can be described by a sum of two exponentials:

$$A_r = A_1 \cdot e^{(x-400\text{cm})/L_1} + A_2 \cdot e^{(x-400\text{cm})/L_2} \quad (1)$$

where $x(\text{cm})$ is the distance of the source from the away side end. The resulting fit is represented by the solid lines. The fit results for the individual strips are summarized in table 2.

Table 2: Fit Results - away-side end: BLACK TAPE						
Scintillator	A_1	L_1 (cm)	A_2	L_2 (cm)	A_2/A_1	χ^2/NDF
1	180±2	284±2	155±5	35±1	0.85	9.1
3	193±4	318±7	87±3	57±4	0.45	8.8
4	232±2	270±2	58±8	28±5	0.25	6.5
6	221±2	232±2	112±14	21±2	0.51	10.1
AV(3,4,6)	220.9±1.2	263.8±1.4	81.6±3.6	28±2	0.37	5.6
7	263±1	195±1	80±9	13±2	0.30	11.9
9	255±1	185±1	72±5	18±1	0.28	14.4
10	272±1	201±1	115±111	8±4	0.43	13.8
AV(7,9,10)	263.1±0.6	193.1±0.5	82±7	12.3±0.8	0.34	23.6

The effect of wrapping the scintillator into white, diffuse reflecting paper was also studied. As expected, this did not alter the response in a noticeable way.

5. Estimate of the Number of Photoelectrons

Fluctuations in the difference of the pulseheight measured with the right and the left PMT on an event by event basis, are expected to be solely due to

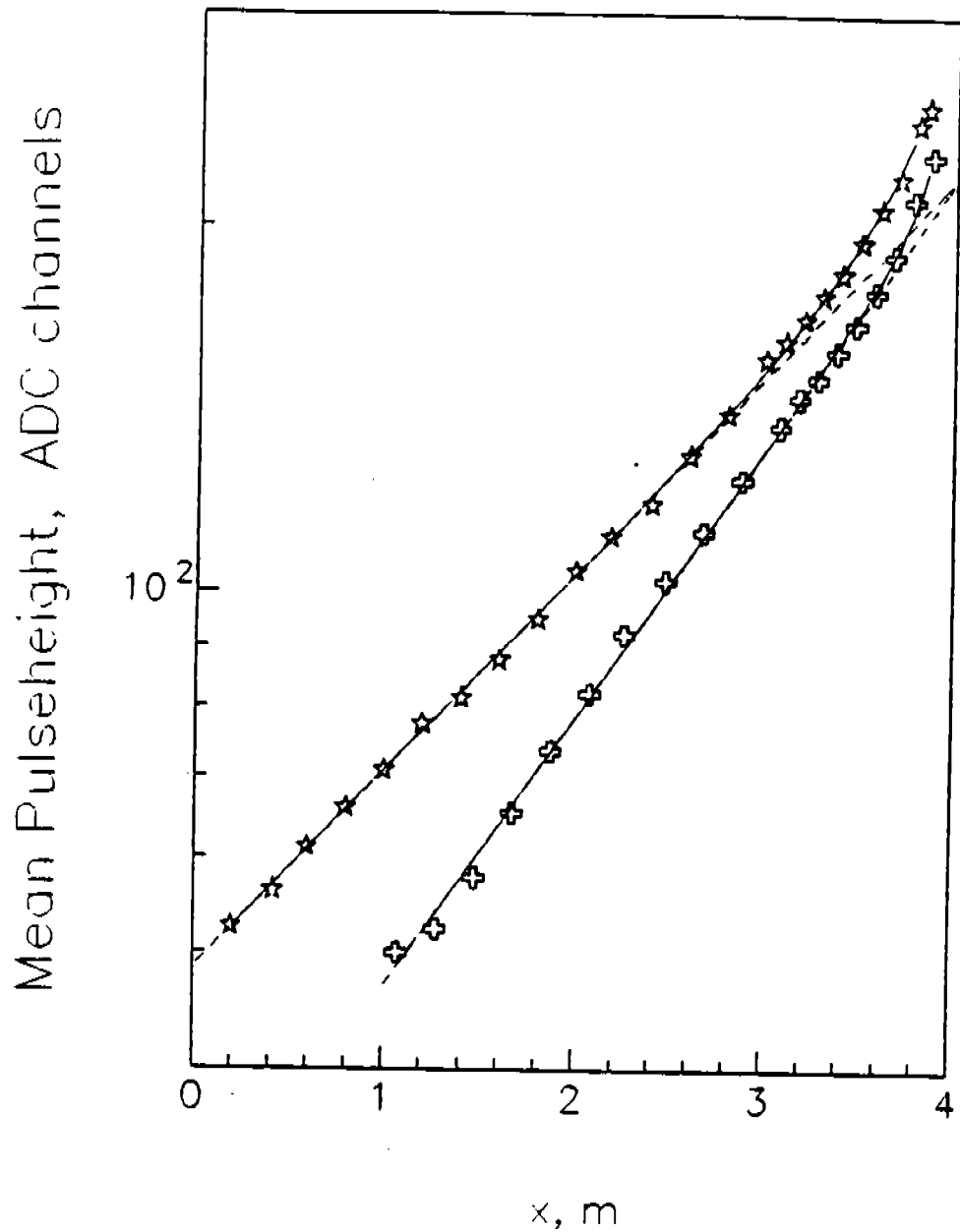


Figure 5: Position dependence of the mean pulseheights. The solid curves represent fits to the data using a formula (1). The asterisks correspond to three averaged 4 m long scintillators and the crosses to the averaged 3.1 m long scintillators. The dashed lines represent the first exponential in (1). The data are normalised to have equal first exponential at $x = 4$ m.

photoelectron statistics. The widths σ_s of the distribution of the asymmetry

$$S = \frac{A_L - A_R}{A_L + A_R} \quad (2)$$

measured in the center of the scintillator bars, is related to the number of photoelectrons generated in the cathodes in the following way (assuming identical performance of the PMT's at both ends):

$$\langle N \rangle_{p.e.} = \frac{2}{\sigma_s^2} \cdot \frac{\delta}{\delta - 1} \quad (3)$$

where δ is the amplification of the first PMT dynode. Figure 6 shows the dependence of σ_s on the source position. Taking σ_s at the center of the strip, and using $\delta = 3$ we obtain values of

$$\langle N \rangle_{p.e.} = 75 - 100$$

for the various scintillator strips. Since the average energy deposition is about 2.0 MeV, we obtain about 37 - 50 photo-electrons per MeV energy deposition. Only about 45% of the scintillator cross section is read out by the PMT. For complete coverage about 80 - 110 photo-electrons per MeV would be generated.

6. Time Characteristics of the Scintillators

The timing properties of the scintillators were studied by measuring the time difference between the left(right) PMT (start) and the probe PMT (stop). The TDC spectra were fitted to Gauss distributions. Figure 7 shows the time difference between the left PMT signal and the probe PMT signal. The corresponding widths (σ) of the measured spectra are shown in Figure 8. The following information can be extracted from this spectra:

- In the center point, $x = L_s/2$, we observe $\sigma_T \sim 500psec$ ($\sim 700psec/\sqrt{2}$) corresponding to $\langle N \rangle_{p.e.} \sim 75$.
- The change in time resolution with increasing distance of the probe PMT from the left PMT cannot be entirely attributed to pulseheight changes (number of photoelectrons). If the pulse shape were preserved a change in the time resolution of $\sqrt{\langle N \rangle_{p.e.}^2 / \langle N \rangle_{p.e.}}$ would be expected.

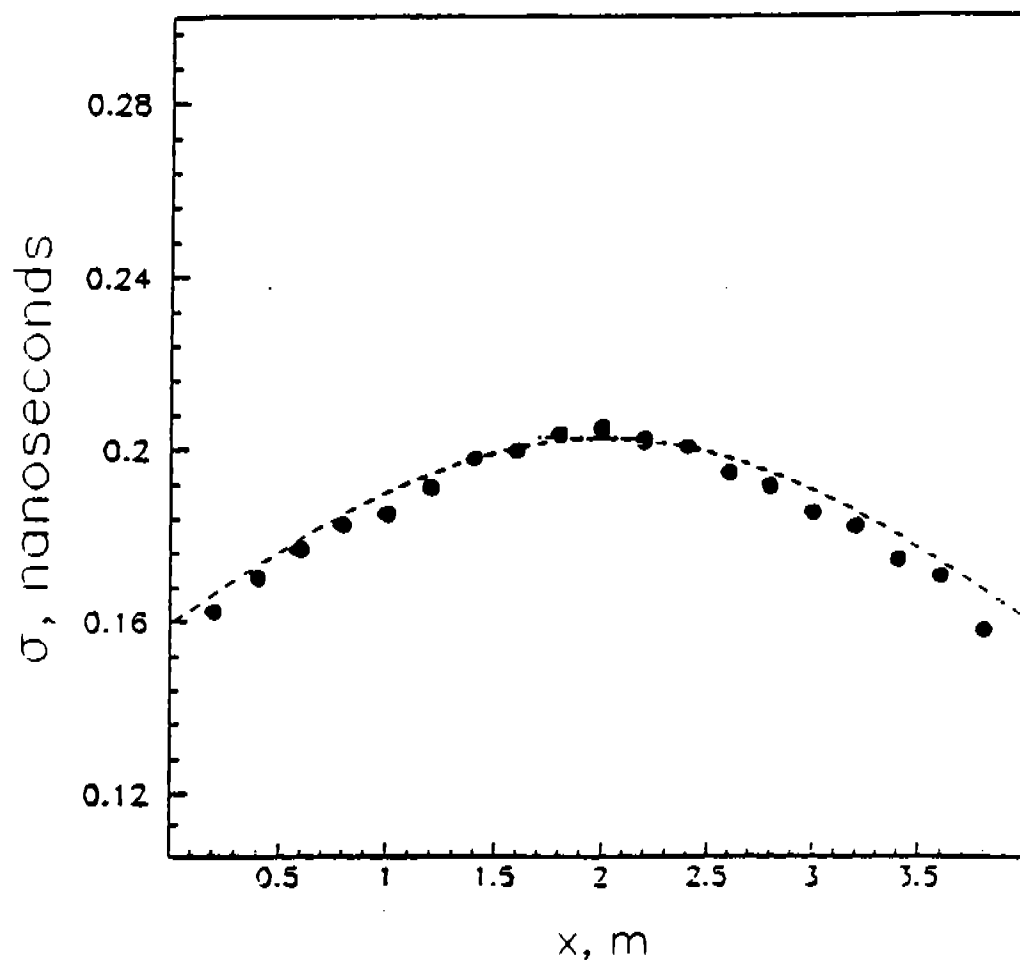


Figure 6: Position dependence of σ .

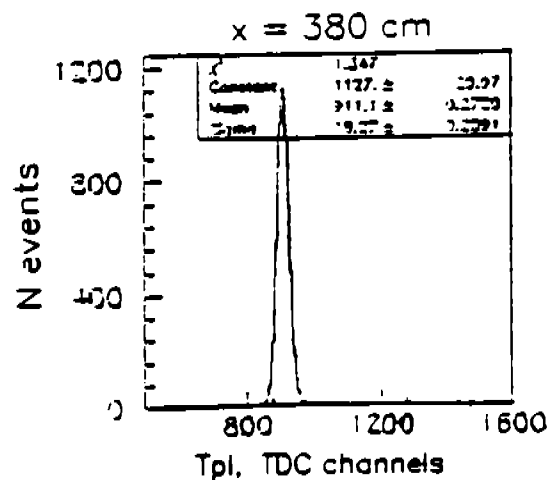
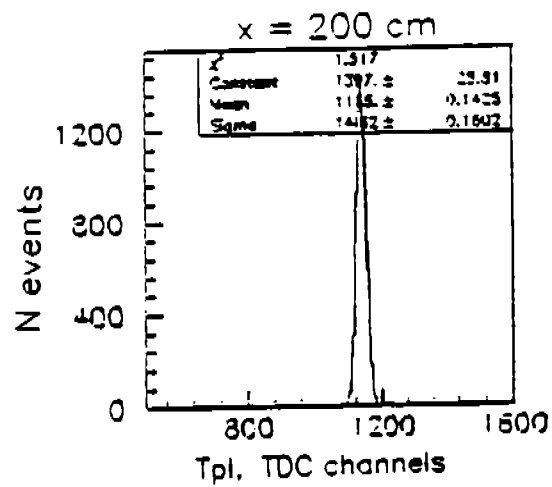
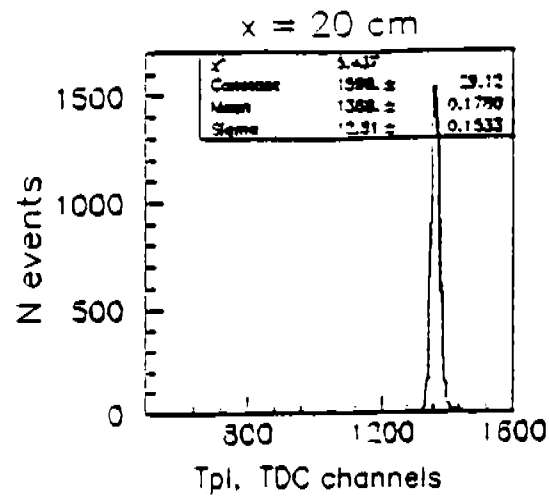


Figure 7: Typical TDC spectra for 3 positions of the source. T_{pl} represents the time difference between the left PMT and the probe PMT. The lines represent Gauss fits.

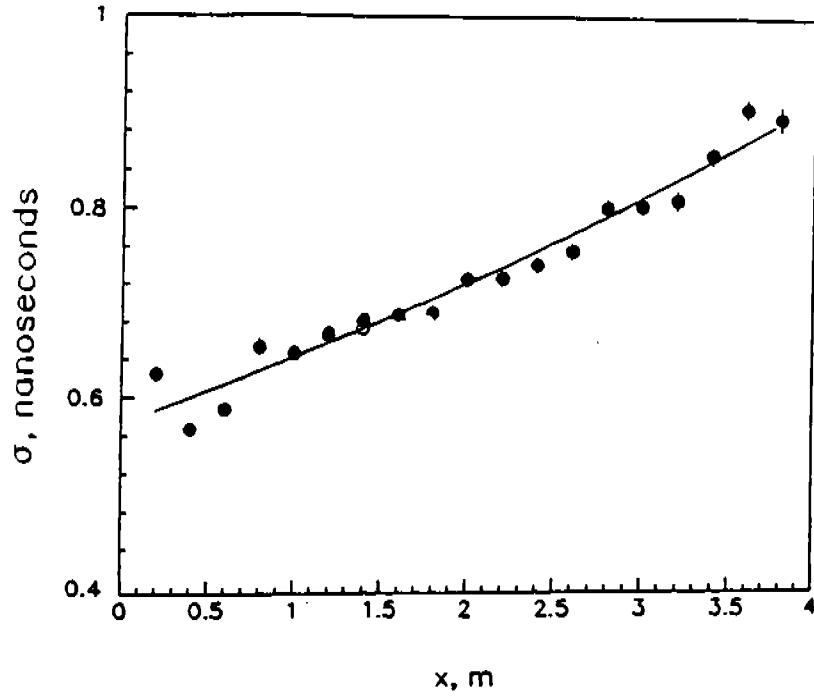


Figure 8: Width (σ) of the measured TDC spectra versus the source position.

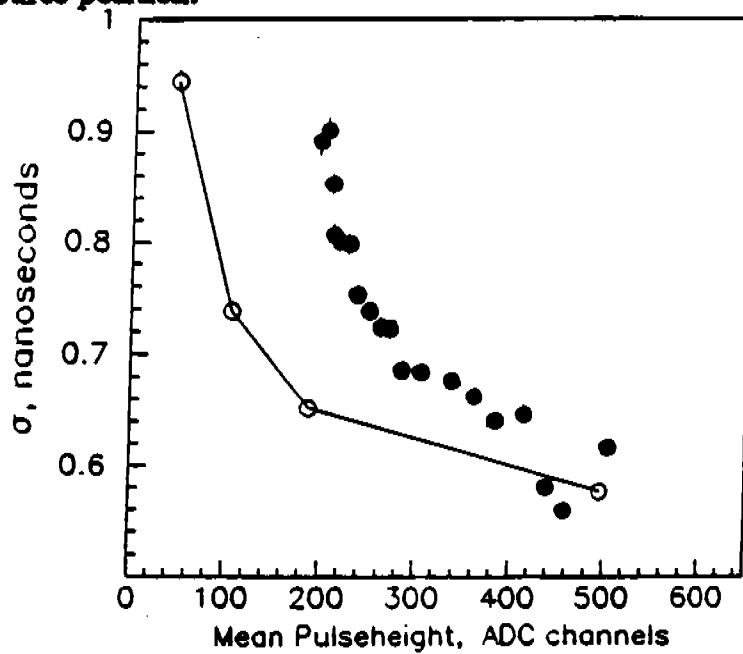


Figure 9: Widths (σ) of the TDC spectra for different source positions (full circles), and near the right PMT but with the pulseheight reduced to the same values using black paper masks (open circles).

However, when going from $x = 20\text{cm}$ to $x = 380\text{cm}$ σ_{pl} increases by a factor of ~ 2.7 , while $\sqrt{\langle N \rangle}_{p.e.}$ decreases only by a factor of 1.6.

The difference in the timing properties may be attributed to time dispersion effects resulting from the increased spread in the light path length with increasing distance from the PMT. In order to estimate this effect, we compare the width of the timing distribution for events at a distance to the PMT, with events near the PMT but with the pulseheight reduced to the same mean value using masks that block out the corresponding amount of light. This is shown in Figure 9. From these data, the contribution of the scintillator to the time resolution is estimated to $\sigma_T \sim 600\text{psec}$ at a distance of 380 cm from the PMT, and to $\sigma_T \sim 300\text{psec}$ at 200 cm.

7. Light Transmission in the Wavelength Shifter Bars

The CLAS electromagnetic calorimeter will be read out by means of wavelength shifter bars (WLS) which absorb the light of an entire stack of scintillator bars. The WLS absorb the blue scintillator light ($\sim 400\text{nm}$) and re-emit it at longer wavelengths (peak $\sim 500\text{nm}$). The absorption and emission spectrum of such a waveshifter is shown in Figure 10.

Two different shapes of waveshifter bars have been tested. WLS-1 had a rectangular geometry with $1 \times 10 \times 50 \text{ cm}^3$ outer dimensions. This bar was glued to a lucite light guide of the same cross section ($1 \times 10 \text{ cm}^2$). The light guide was twisted towards one end to form an approximate cylinder. This end was glued to a cylindrical light guide of 40mm diameter, which was coupled to the PMT using optical grease.** The second waveshifter bar WLS-2 was twisted on one end to form a cylinder which was then coupled to the PMT via the lucite cylinder, this way eliminating one glue joint.

Figure 11 shows the attenuation performance of the rectangular WLS bar for various treatments of the 'away side' end of the bar (opposite to the PMT).

In order to minimize contributions to the energy resolution due to light fluctuation the waveshifter response should be uniform across the full width of the bar. The response across the width of the waveshifter bar are summarized in Figure 12. The data indicate an excellent uniformity across the full 10 cm width.

The attenuation performance and the results of the non-uniformity measurements of the twisted waveshifter are shown in Figure 13 and Figure 14.

** Bicron BC 630

BC - 482A Wavelength Shifter

Absorption and Emission Spectra

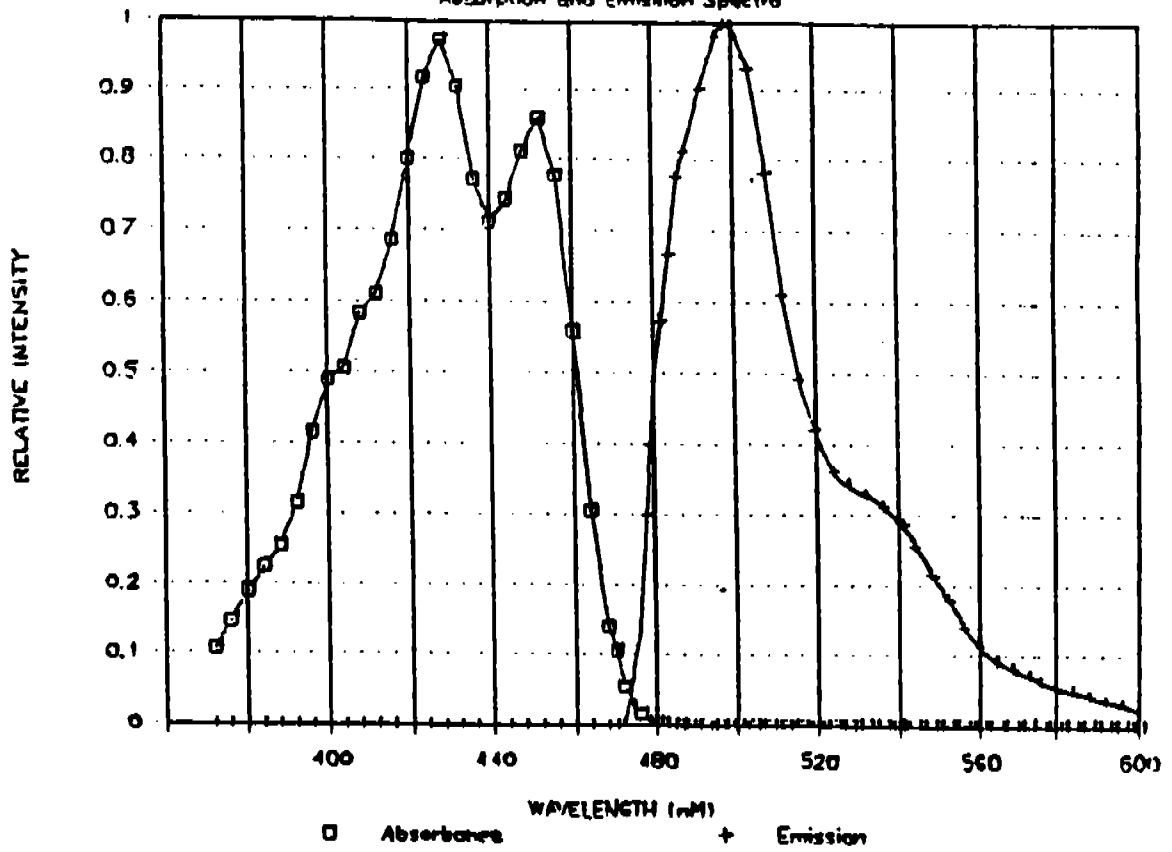


Figure 10: Typical absorption and emission spectrum of the wavelshifter material (e.g. BC 482A or NE 172).

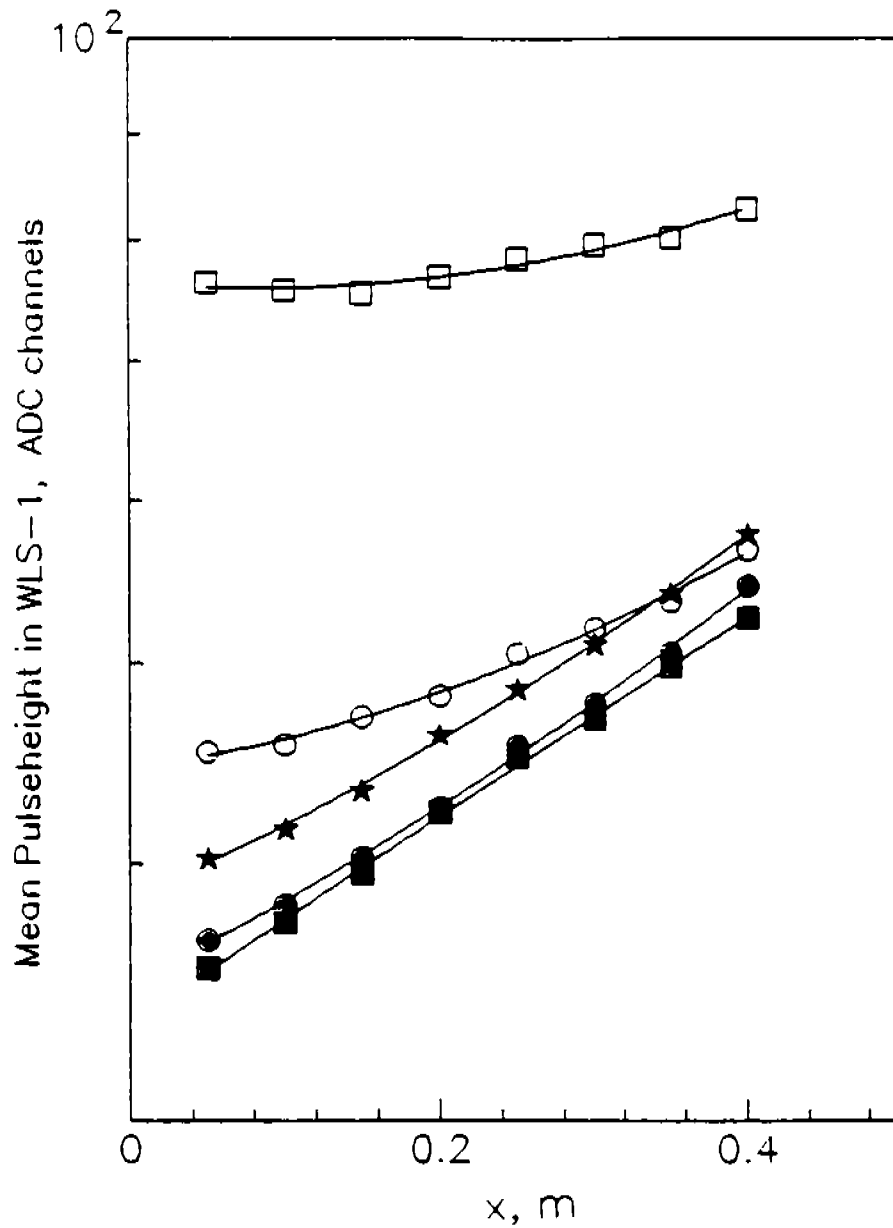


Figure 11: Attenuation performance of the rectangular wavelength shifter bar for various treatments of the away-side end. Open end (open circles), reflective aluminized mylar foil (open squares), black tape (full circles), black paint coating (full squares). Black paint coating with light guide wrapped in aluminized mylar (asterisk).

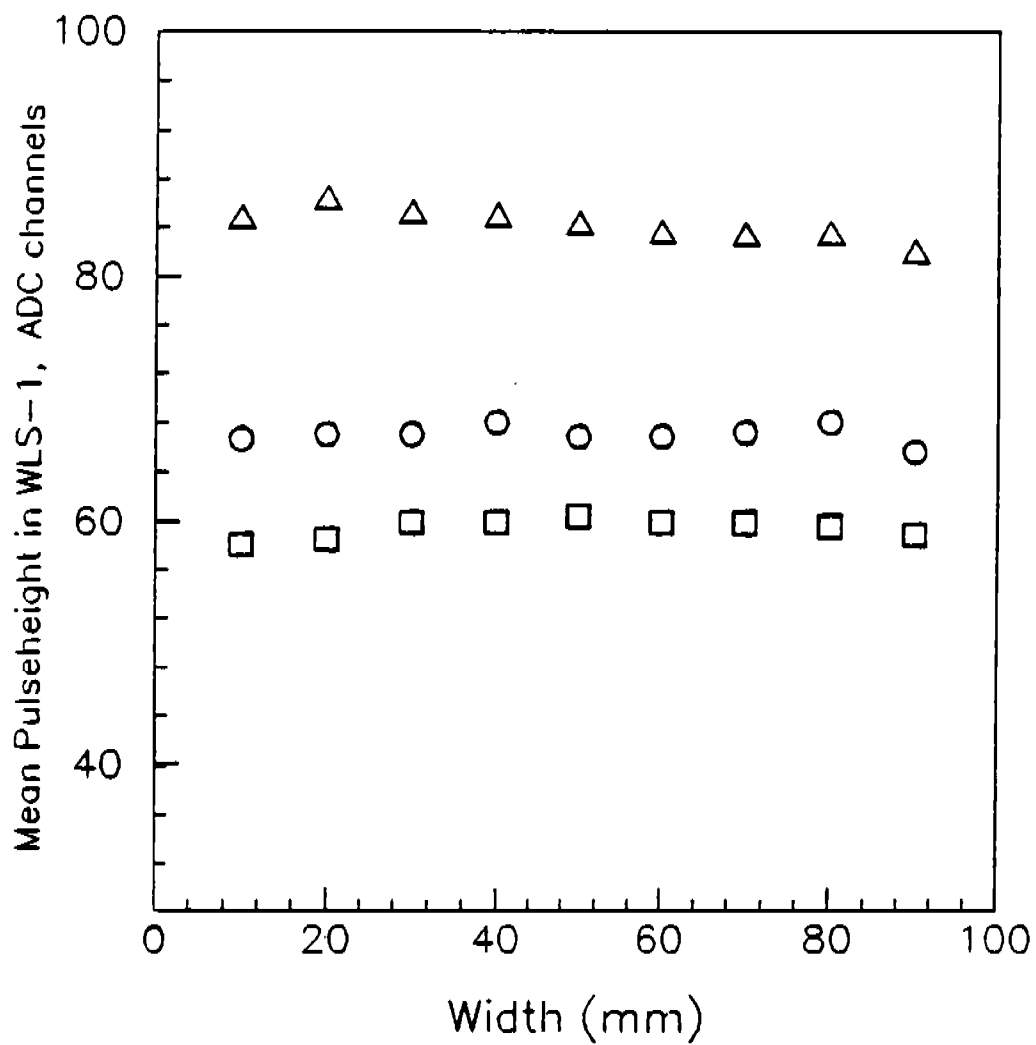


Figure 12: *PMT response for various positions of the radioactive source across the waveshifter width for various distance from the away-side end; 1 cm (squares), 25 cm (circles), 50 cm (triangles)*

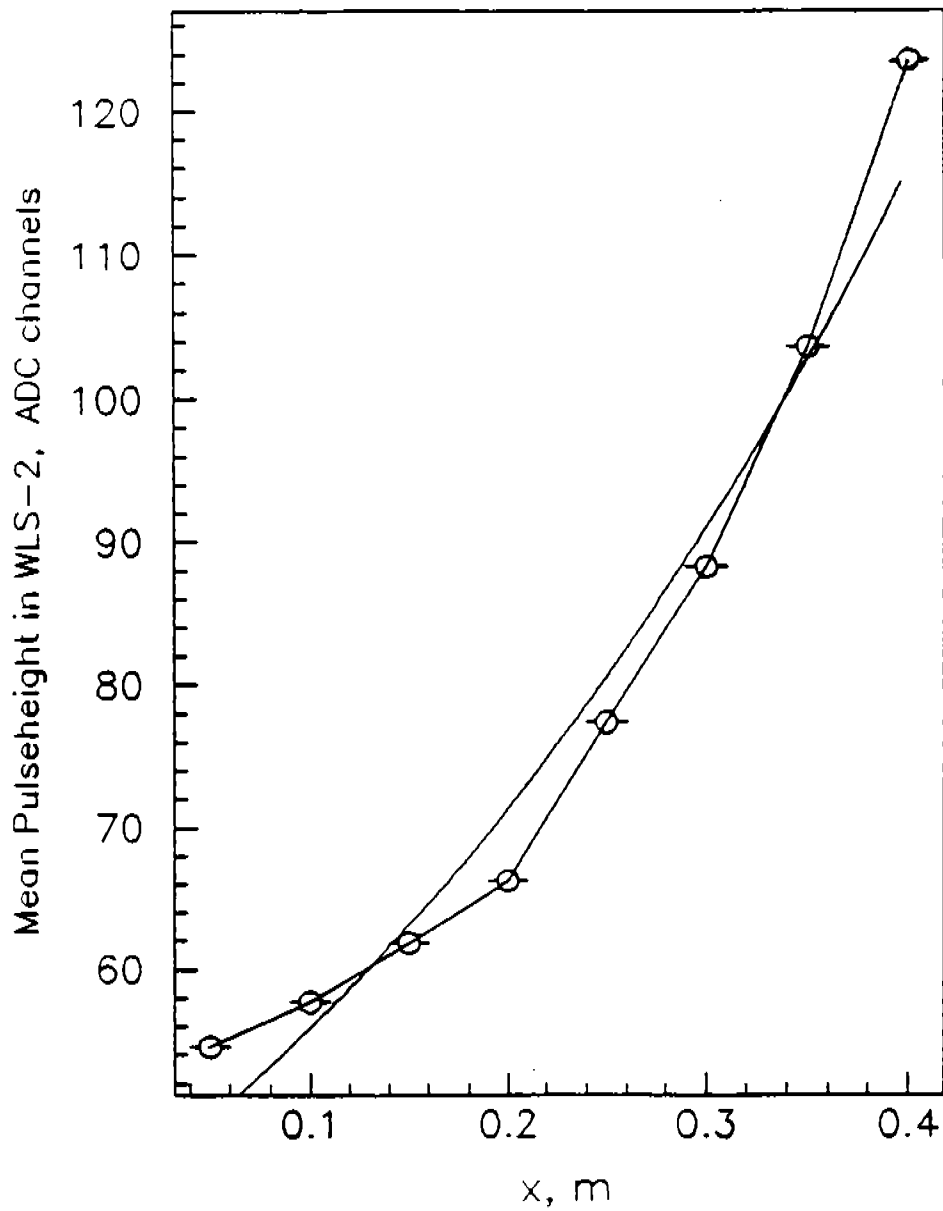


Figure 13: Attenuation performance of the twisted waveshifter; away-side end: open.

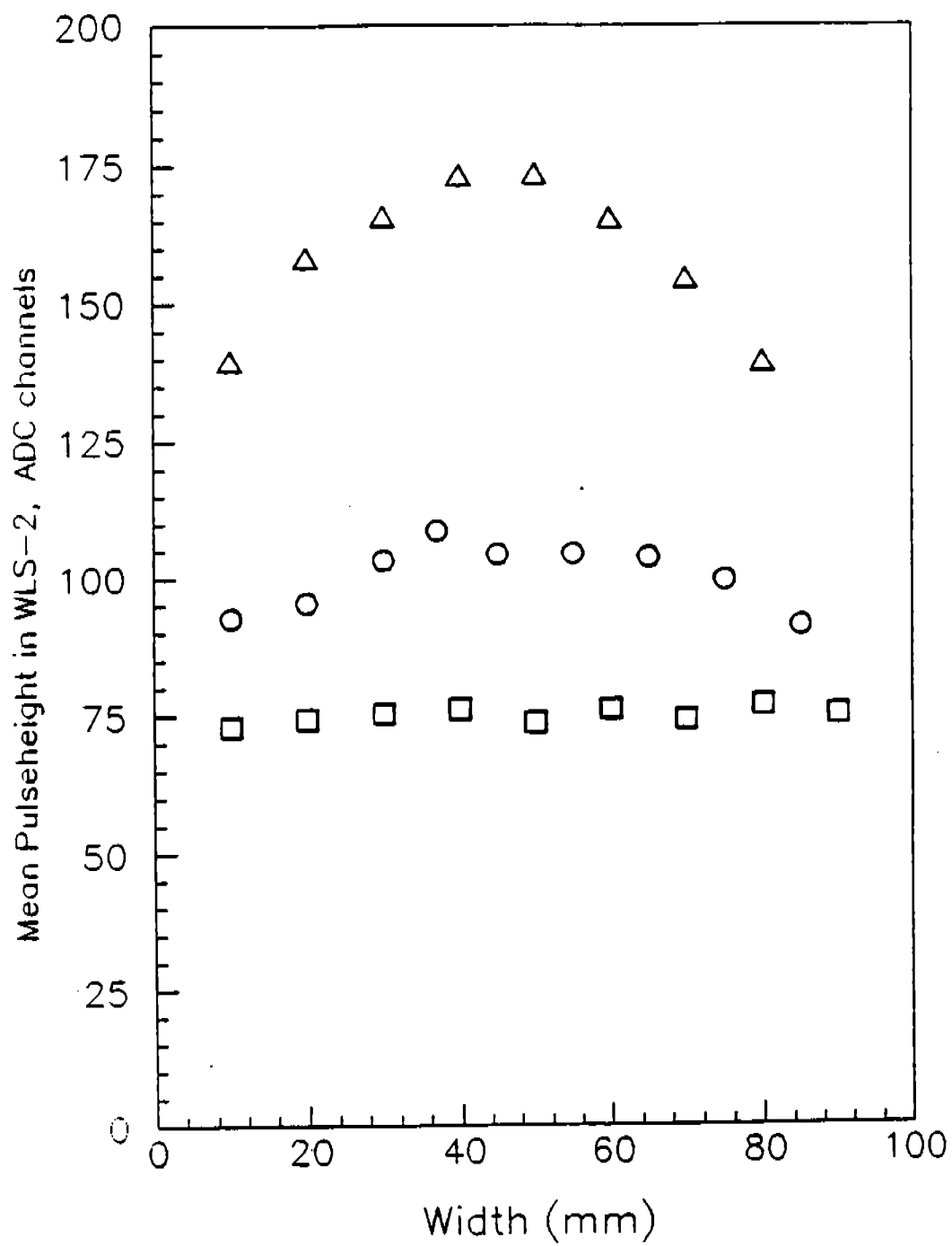


Figure 14: PMT response for various positions of the radioactive source across the width of WLS-2 for various distance from the away-side end; 1 cm (squares), 20 cm (circles), 38 cm (triangles).

In this case a significant non-uniformity in the response occurs when the source is located near the region where the twisting of the waveshifter bar begins. To make the response more uniform over the entire readout region the waveshifter would have to be extended.

8. Time Characteristics of the Wavelength Shifter Bars

In order to measure the time characteristics of the waveshifter lightguide WLS-2, the waveshifter was positioned perpendicular to the scintillator strip at a distance of ~ 1 mm. Light generated in the scintillator was transmitted to the waveshifter through this air gap. Light absorbed and re-emitted in the waveshifter was transported to the PMT which was coupled to the waveshifter via a lucite cylinder. The lucite cylinder was glued directly to the waveshifter, and attached to the PMT with optical grease.

One end of the WLS was covered with an aluminized mylar foil. This led to an increase of the light yield by a factor of 1.8. The surface opposite to the scintillator strip was also covered by aluminized foil which increased the yield by another 10%. The probe counter was used to select a 2.0 ± 0.3 MeV energy deposited in the scintillator strip. The probe and the radioactive source were positioned at a distance of 20 cm from the WLS, close to the end of the WLS bar. The pulseheight distribution is shown in Figure 15. It is well described by a Poisson distribution with $\langle N \rangle \sim 7$. Folding in the amplification of the first dynode according to equation (3) we obtain $\langle N \rangle_{p.e.} \sim 10.5$, corresponding to $\langle N \rangle_{p.e.} \sim 5$ MeV⁻¹.

In order to measure the decay time of the WLS we reduced the amount of light passing from the scintillator to the WLS by a factor of ~ 10 . This was achieved by screening the WLS from the scintillator with strips of black tape. As a result, the number of photoelectrons in the PMT was reduced to $N_{p.e.} \sim 0.7$. This enabled us to sample the decay distribution of the WLS. The resulting time distribution is shown in Figure 16. The rising edge can be described by a Gaussian with $\sigma \sim 2.2$ nsec, and the fall-off is well described by an exponential with a time constant of 7.47 ± 0.11 nsec.

Acknowledgements

We want to thank Don Joyce and Bogdan Niczyporuk for their help in the data handling.

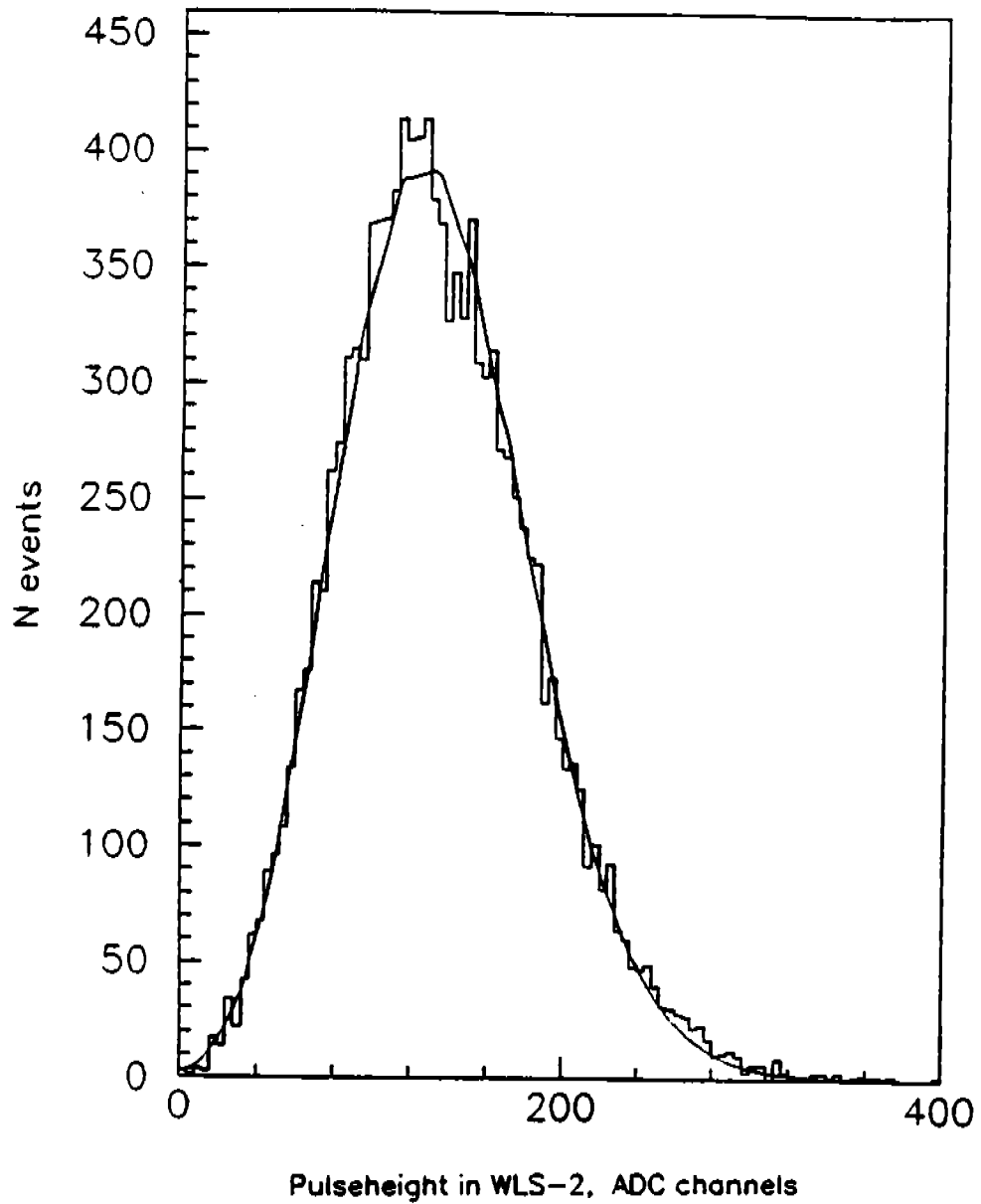


Figure 15: Pulseheight distribution in WLS-2 waveshifter. The solid line represents fit to a Poisson distribution.

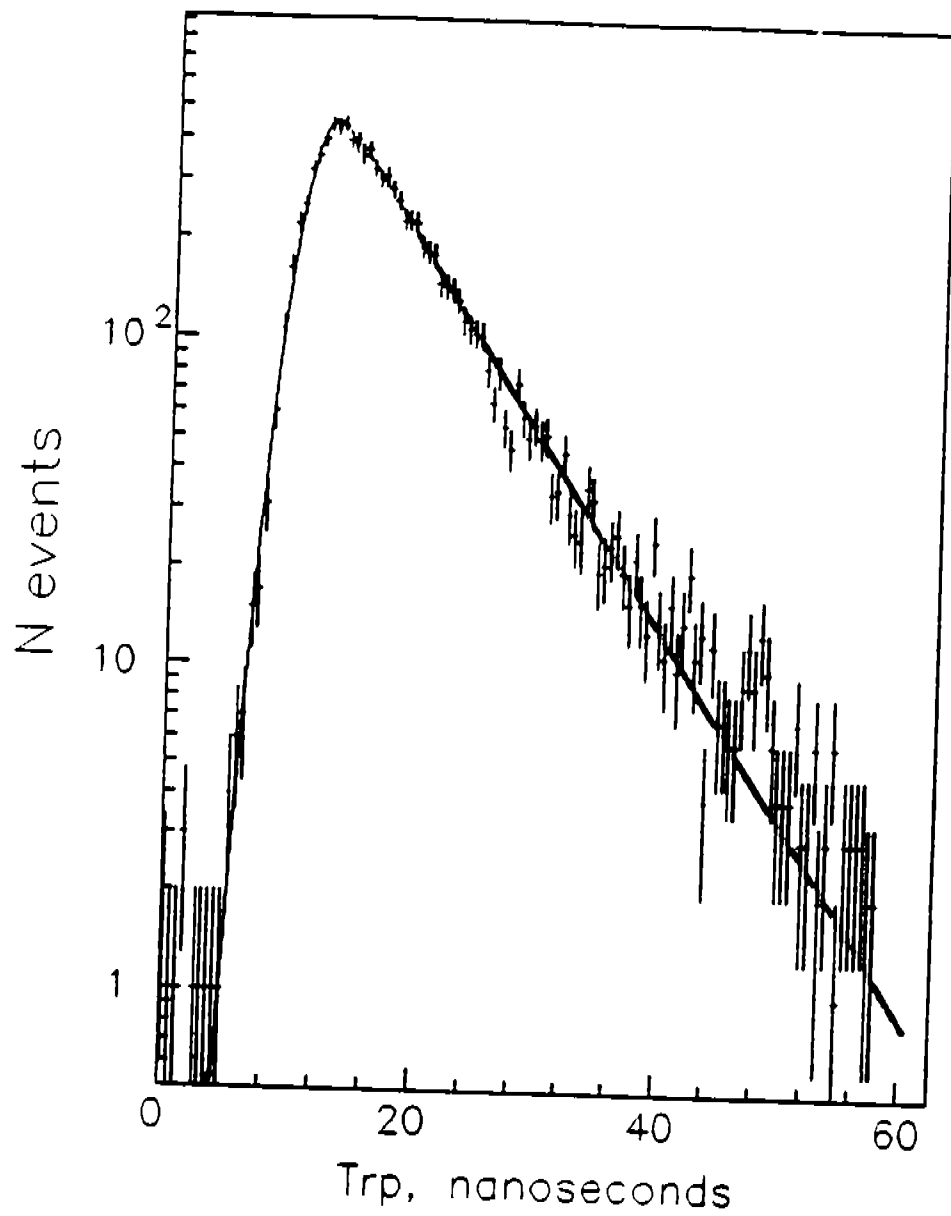


Figure 16: The decay time distribution of WLS-2 waveshifter. The solid lines represent fits of the rising edge to a Gaussian and the fall-off to an exponential distributions.

References.

- [1] CEBAF Conceptual Design Report - Basic Experimental Equipment, April 1990
- [2] PAW - Physics Analysis Workstation, R. Brun et al., October 1989, CERN.